Food Chemistry: X 25 (2025) 102080

Contents lists available at ScienceDirect

Food Chemistry: X

journal homepage: www.sciencedirect.com/journal/food-chemistry-x

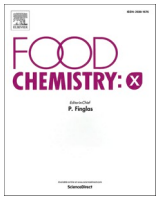

Enhanced stability and oxidation resistance of *Acer truncatum* Bunge seed oil Pickering emulsion using rice bran protein modified by phytic acid

Jianjun Huang, Ruyi Sha *, Jing Dai, Zhenzhen Wang, Min Cai, Xianxiu Li, Jianwei Mao

School of Biological and Chemical Engineering, Zhejiang University of Science and Technology, Hangzhou 310023, China

ARTICLE INFO

Keywords:
Acer truncatum Bunge seed oil
Pickering emulsion
Rice bran protein
Phytic acid

ABSTRACT

The potential applications of *Acer truncatum* Bunge seed oil in the food and medical industries are constrained by its susceptible fatty acid composition, which is prone to oxidation. In this study, rice bran protein (RBP) was employed as an emulsifier for the fabrication of *Acer truncatum* Bunge seed oil Pickering emulsion. The impact of antioxidant-phytic acid (PA) on the stability of Pickering emulsion and the underlying mechanisms were further investigated. The findings indicate that PA is capable of interacting with RBP, resulting in a change in its spatial conformation. When the PA concentration was increased from 0 to 0.01 % (*w/v*), the number of α-helices of RBP-PA particles decreased by 5 %, the number of β-sheets and interfacial adsorbed proteins increased by 2.89 % and 39.83 %. Additionally, and the surface hydrophobicity was increased from 50 ± 3.63 (a.u.) to 429 ± 20.03 (a.u.), and the range of the particle size distribution was reduced from 1 to 10 μm to 295–459 nm, and the zeta potential decreased from −23.43 ± 0.46 mV to −53.4 ± 1.35 mV. The *Acer truncatum* Bunge seed oil Pickering emulsion, containing 0.01 % PA, exhibits favourable static stability and lipid oxidative stability, allowing for storage at room temperature for a period exceeding 50 days.

1. Introduction

Acer truncatum Bunge is a diploid monoecious tree species belonging to the Aceraceae family, originates from northern and western China and is currently cultivated extensively across the globe. The oil content of *Acer truncatum* Bunge seeds ranged from 17.81 % to 36.56 %. The seeds contain 52.81 % monounsaturated fatty acids, of which 5–6 % is nervonic acid, and 39.2 % polyunsaturated fatty acids, specifically 37.35 % linoleic acid (omega-6) and 1.85 % linolenic acid (omega-3) (Qiao et al., 2019; Yang, Zhang, Li, Yu, & Zhang, 2018). Nervonic acid is an important member of the functional very long-chain monounsaturated fatty acid. It is closely related to the development and maintenance of the brain and the biosynthesis and improvement of nerve cells (Li, Chen, Yu, & Gao, 2019). Moreover, *Acer truncatum* Bunge seed oil (ATBSO) is rich in lipid concomitants such as tocopherols. However, the fat-solubility of both ATBSO and its beneficial components poses limitations on their application in water-soluble foods, pharmaceuticals and other areas (Qi et al., 2023).

As an encapsulated transport system, food-grade O/W Pickering emulsions have been widely employed in food processing, drug delivery and two-phase bioreactor construction (Guo et al., 2024). This is due to their ability to promote the water solubility of fat-soluble substances, improve the stability and bioavailability of actives and modulate interparticle interactions, thereby meeting the requirements of a range of applications (Yan et al., 2020). Protein nanoparticles exhibits significant advantages in the formulation and stabilization of Pickering emulsion, thanks to their the abundant raw materials, ease of extraction, biodegradability, biocompatibility, excellent nutritional value and outdtanding surface activity (Zhang et al., 2021). Rice is one of the most widely consumed food crops globally (Li, Liang, Lu, Liu, & Wang, 2024). Rice bran protein (RBP) is a low-cost, nutritionally dense by-product of rice processing, containing 18 amino acids, including 8 of them being essential. Furthermore, RBP is hypoallergenic and can be used in food formulations for individuals with specific dietary requirements, such as infants and the elderly, which is a prerequisite and a significant advantage for its potential application in the field of food-grade Pickering emulsions. However, because of its molecular structure and weight constraints, RBP cannot sufficiently swollen, dispersed, and rearranged at the O/W interface (Chen, Ding, Zhao, & Ma, 2023). Additionally, the O/W Pickering emulsion formulated with vegetable oil is vulnerable to lipid oxidation during both food processing and storage phases, largely due to the specific characteristics of their fatty acid composition.

* Corresponding author.
E-mail address: rysha@zust.edu.cn (R. Sha).

https://doi.org/10.1016/j.fochx.2024.102080
Received 20 August 2024; Received in revised form 17 November 2024; Accepted 8 December 2024
Available online 9 December 2024

Phytic acid (PA), a naturally occurring substance abundant in rice bran and other fibre-rich plants, comprises six phosphate groups attached to an inositol ring, which provides 12 negative charges and has the ability to chelate metal ions or proteins directly or indirectly. The distinctive chemical configuration of PA not only confers antioxidant properties but also exhibits physiological benefits, including anticancer effects, blood sugar regulation, and the facilitation of anthocyanin absorption (Cui et al., 2023). Furthermore, it has been demonstrated that PA can enhance emulsion stability by modulating the colloidal interactions between particles (Wang & Guo, 2021). When compared to other modification methods, the utilisation of PA-protein interactions to regulate the assembly behaviour and enhance the functional attributes of food components, and to prepare bespoke structured and functionalised foods, is a more straightforward, environmentally friendly, secure and manageable process. Nevertheless, the interfacial behaviour of PA-RBP particles stabilizing the *Acer truncatum* Bunge seed oil Pickering emulsion and the mechanism of action remain unclear.

In this study, rice bran protein-*Acer truncatum* Bunge seed oil Pickering emulsion (RAe) and rice bran protein-phytic acid-*Acer truncatum* Bunge seed oil Pickering emulsion (RPAe) were prepared. We then conducted a comparative analysis to investigate the potential of PA in improving the stability of Pickering emulsions and the lipid oxidation stability, while elucidating the interaction between PA and RBP. This study aims to address the issue of PA antinutrition and make effective use of its functional properties from the vantage point of food component interactions. It also seeks to establish a foundation for the development of stable *Acer truncatum* Bunge seed oil emulsion and related dairy products.

2. Materials and methods

2.1. Materials

Acer truncatum Bunge seed oil (ATBSO, 99 % pure) purchased from Sanxi Nanba Biotechnology Co., Ltd. (Shanxi, China). Rice bran protein (RBP, 97 % pure) purchased from SXBC Kangze Biotech Co., Ltd. (Shanxi, China). Phytic acid (PA, 50 % pure) purchased from Tongxiang Xinrui Biotechnology Co., Ltd. (Zhejiang, China). Other chemicals were of analytical grade.

2.2. Preparation of Pickering emulsion

The 3 % (*w/v*) solution of RBP was prepared by dispersing a specific mass of RBP powder in ultrapure water with continuous stirring until completely dissolved. Following this, the solution was then stored at 4 °C overnight to ensure thorough hydration of the protein. Additionally, The 1 % (*w/v*) PA solution should be prepared by diluting the 50 % (*w/v*) PA solution with ultrapure water and used immediately after preparation.

Preparation of RBP-PA mixed solution: The 3 % (*w/v*) fully-hydrated RBP stock solution and the 1 % (w/v) PA solution were combined and diluted with ultrapure water, resulting in a mixed solution with the RBP concentration of 0.05 % (w/v) and the PA concentration of 0.005 %, 0.01 %, 0.02 %, 0.04 %, and 0.08 % (w/v), respectively. In that order, with the total volumes of the samples remaining consistent across varying ratios. The final pH of the mixtures was adjusted to 8 using 1 mol/L NaOH. Following this, ATBSO was then added to the resulting mixed solution at 10 % (*v*/v). Initially, coarse Pickering emulsion was prepared using a shear homogenizer (model T-18DS25, IKA Ltd., German) at 8000 rpm for 2 min. Afterwords, fine Pickering emulsion was obtained by using an ultrasonic crusher (model FS-750 T, Ultrasonics Instruments Co., Ltd., Shanghai, China) at 50 % output power (rated power 750 W) for 6 min.

2.3. Determination of microstructure

The freshly prepared Pickering emulsion micro-structure was observed through a fluorescence micro-imaging microscope (model BX53F, Olympus Co., Ltd., Japan). The fat droplets in 300 μL of Pickering emulsion were stained with 20 μL of a nile red ethanol solution (1 mg/mL). A 10 μL aliquot of the stained Pickering emulsion was placed on a microscope slide, covered with a coverslip to prevent evaporation, and subsequently the sample was observed with an inverted fluorescence microscope.

2.4. Determination of particle size and zeta potential

The mean particle size and zeta potential were determined by Malvern Zetasizer Nano Series (model ZEN3600, Malvern Panalytical Instruments Ltd., UK) at 25 °C. The samples were uniformly dispersed in phosphate buffer solution (PBS, pH 8.0), and the dilution volume fraction was 1:100. The refractive indices of the oil and water phases were 1.495 and 1.33. All the determinations were conducted in triplicate.

2.5. Determination of percentage of adsorbed proteins

To determine the percentage of adsorbed protein (AP) on surface of Pickering emulsion, the reported method by Peng et al. was followed with minor modifications (Peng et al., 2016). The Pickering emulsion was subjected to centrifugation at 12000 r/min for 20 min. The aqueous phase was then collected using a syringe and centrifuged three times to remove the emulsion layer. The final aqueous phase was collected, and the protein content was determined using the Bradford method. The percentage of adsorbed protein (AP%) was calculated using the formula below:

$$AP(\%) = (C_1 - C_2)/C_1 \times 100\% \quad (1)$$

The protein concentration in the Pickering emulsion initially is denoted by C_1 (g/mL), whereas C_2 (g/mL) signifies the protein concentration in the aqueous phase of the Pickering emulsion.

2.6. Determination of the emulsification properties

The emulsifying activity index (EAI) and emulsification stability index (ESI) of the Pickering emulsion were determined following reported methods (Wang et al., 2023). Specifically, 50 μL of the sample was taken and diluted 100 times using a 0.1 % sodium dodecyl sulphate (SDS) solution. The initial absorbance A_0 was measured at a wavelength of 500 nm. After standing for 10 min, the supernatant was removed to determine the absorbance A_{10}. The EAI and ESI were then calculated as follows:

$$EAI\left(m^2/g\right) = \frac{2 \times 2.303 \times \omega \times A_0}{10000 \times \theta \times C} \quad (2)$$

$$ESI(min) = \frac{A_0}{A_0 - A_{10}} \times (T_{10} - T_0) \quad (3)$$

The protein concentration (g/mL) is represented by C, while the dilution multiple of 100 is represented by ω. The volume fraction of oil (0.1) is represented by θ. A_0 and A_{10} represent the absorbance at 0 min and 10 min, respectively. T_0 refers to 0 min and T_{10} refers to 10 min.

2.7. Determination of lipid oxidation

Lipid oxidation was determined following previously reported method (Pei, Deng, McClements, Li, & Li, 2020). Initially, 0.3 mL of the Pickering emulsion was mixed with 1.5 mL of octane/isopropanol (3,1, *v*/v). Following this, the mixture was centrifuged at 8000 rpm for 15 min. After centrifugation, 0.2 mL of the supernatant were collected and combined with 2.8 mL of methanol/1-butanol (2,1, v/v). Then, 15 μL of

a ferrous solution (consisting of 0.132 mol/L $BaCl_2$ and 0.144 mol/L $FeSO_4$, in a 1:1, v/v ratio) and 15 μL of ammonium thiocyanate (3.94 mol/L) were added. The resulting solution was kept in darkness for 20 min, and its absorbance was measured at 510 nm. The peroxide value (POV, mmol/kg lipid) was calculated using standard curves prepared with cumene hydroperoxide.

0.25 mL of the Pickering emulsion was added to 0.75 mL of water and then mixed with 2.0 mL of thiobarbituric acid (TBA) reagent (containing 15 g trichloroacetic acid, 0.375 g TBA, 1.76 mL of 12 mol/L HCl and 82.9 mL of H_2O). The mixture was sealed in a test tube and placed in a 95 °C water bath for 15 min. Afterward, it was sonicated for 20 min and centrifuged at 3000 rpm for 20 min. The absorbance of the supernatant was measured at 532 nm. To determine the thiobarbituric acid reactive substances (TBARS, mmol MDA/mL) content, standard curves were prepared with 1,1,3,3-tetraethoxypropane.

2.8. Evaluation of Pickering emulsion stability

pH stability: The pH of the freshly prepared Pickering emulsion was adjusted to 5–10 with 1 mol/L NaOH and HCl, and the particle size was determined after 24 h of standing at room temperature.

Ionic strength stability: The ionic strength of the freshly prepared Pickering emulsion was adjusted by the addition of varying masses of NaCl, resulting in a range of 0–400 mM. The average particle size was then determined after 24 h of standing at room temperature.

Thermal stability: The freshly prepared Pickering emulsion was subjected to different temperature conditions (0–80 °C), and the average particle size was determined after a seven-day period.

2.9. Morphological characterization

The RBP-PA composite particles were obtained after freeze-drying treatment of the RBP-PA mixture solution obtained in 2.2 with a vacuum freeze-dryer (model FreeZone 2.5, Labconco Ltd., USA). The composite particles were affixed with a conductive adhesive tape placed on a stainless steel stage. The surplus powder was meticulously removed with a washing ball and positioned within an ion sputtering apparatus for vacuum gold spraying. The microstructure of the samples was then examined under a current intensity of 10 mA and an accelerating voltage of 5KV using a scanning electron microscope (model S-4800, Hitachi Ltd., Japan).

2.10. Determination of surface hydrophobicity

Surface hydrophobicity (H_0) was determined following the reported method (Wang et al., 2023) with minor modifications. The samples were diluted in PBS (10 mmol/L, pH 8.0) to achieve concentrations of 0.05, 0.1, 0.15, 0.2, and 0.25 (mg/mL). Subsequently, 4 mL of each diluted sample was mixed with 40 μL of the fluorescent probe 8-Anilino-1-naphthalenesulfonic acid (ANS, 8 mmol/L), and then kept away from light for 15 min. The fluorescence intensity of the samples was measured using a multifunctional enzyme labeller (model SpectraMax iD3, Molecular Devices Ltd., USA). The test parameters were set to an excitation wavelength 390 nm, and an emission wavelength 470 nm. The fluorescence intensity measurements were plotted as the ordinate, with the sample protein concentration as the abscissa, and the initial slope representing the sample's H_0 value.

2.11. Endogenous fluorescence assay

The endogenous fluorescence spectra of samples were measured using a fluorescence spectrophotometer (model F-4500, Hitachi Ltd., Japan). The excitation wavelength was set to 280 nm, while the emission wavelength spanned from 250 to 500 nm. Both excitation and emission slit widths were maintained at 5 nm, and the scanning speed was adjusted to 1200 nm/min.

2.12. Fourier transform infrared (FT-IR) spectroscopy

The FT-IR spectra of lyophilised RBP-PA complexes were measured using a Fourier infrared spectrometer (model VERTEX 70 V, Bruker Optics Ltd., Germany). The samples, along with KBr, were mixed and pressed in a 1:100 (*w*/w) ratio at an assay temperature of 25 °C. IR spectra were recorded with a resolution of 4 cm^{-1} in the spectral range of 4000–400 cm^{-1}. Using the Peakfit v4.12 software, spectra's amide I band (1600 cm^{-1}–1700 cm^{-1}) of the FT-IR spectra underwent detailed analysis. The individual peaks representing the secondary structure of proteins were decomposed into β-sheet (1600–1640 cm^{-1}), random coil (1640–1650 cm^{-1}), α-helix (1650–1660 cm^{-1}), and β-turn (1660–1700 cm^{-1}) (Xie et al., 2022).

2.13. Molecular docking

The crystal structure of the model protein (PDB ID: 1RZL) was obtained from the Protein Data Bank (PDB) (https://www.rcsb.org/). Using Pymol software (version 2.6.0a0 Open-Source, Schrödinger Inc., USA), multiple protein conformations, including protonation and solvent water molecules were removed. The chemical structural formulae of PA were obtained from the PubChem database (https://pubchem.ncbi.nlm.nih.gov/) and pre-processed for structure optimization using AutoDockTools software (version 1.5.7, The Scripps Research Institute, California, USA).

2.14. Statistical analysis

The experiment was conducted at least three times, and the collected data were analysed using SPSS software (version 25.0). The results are reported as mean ± standard deviation. Significant differences between the data were identified using one-way analysis of variance (ANOVA) and at least significant difference (LSD) test at $p < 0.05$.

3. Results and discussions

3.1. Characterization of Pickering emulsion

3.1.1. Macro- and micro-morphology of Pickering emulsion

Fig. 1A show the macroscopic appearance of the Pickering emulsion. After being left at room temperature for 50 days, the colour of RAe turned clear and transparent, signifying the complete separation of oil and water. However, RPAe still showed a significant amount of emulsion. Notably, when the PA concentration was maintained at 0.01 % (*w*/*v*), the Pickering emulsion remained unstratified. The microstructure of the Pickering emulsion (Fig. 1B) demonstrated that the droplet size of RPAe was diminished and the degree of aggregation was reduced in comparison to RAe. This was most notably observed when the concentration of PA was at 0.01 %, resulting in droplets of uniform size without any aggregation or flocculation.Typically, smaller droplets are more resistant to gravitational separation and aggregation than larger ones (Yan et al., 2020). This indicates that PA effectively improved the storage stabilities of *Acer truncatum* Bunge seed oil Pickering emulsion. Additionally, fluorescence microscopy results revealed that the Pickering emulsion consisted spherical oil droplets (coloured red) and Pickering emulsion types were all of O/W type.

3.1.2. Particle size and zeta-potential in Pickering emulsion

Particle size and zeta-potential are two crucial indicators for assessing the stability of Pickerng emulsion. The particle size distribution of freshly prepared RAe and RPAe was shown in Fig. 1C. The particle sizes ($d_{4,3}$) of RAe obtained by ultrasonic homogenisation were found to fall between 1 μm and 10 μm, aligning with the values reported in previous studies (Sun, Lv, Chen, & Wang, 2019). The range of RPAe particle size distributions is less extensive than that of RAe. As the concentration of PA increased, the average particle size of RPAe initially

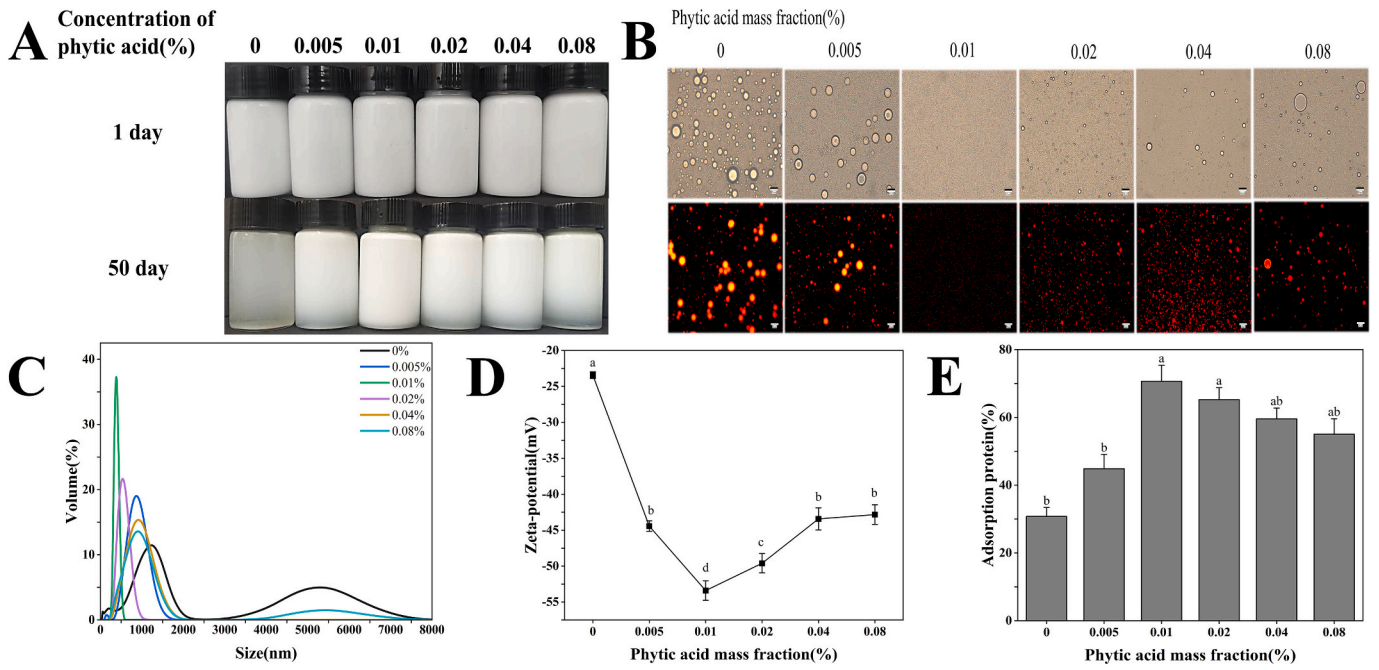

Fig. 1. Macroscopic images of Pickering emulsion stored at 25 °C for 50 day (A), Light and fluorescence microscopy images of Pickering emulsion (B), Particle sizes distribution (C), Zeta-potential (D), Adsorption protein (E). The bars represent 20 μm in scale of (B).

showed a decrease trend, followed by a subsequent upward. When the PA concentration is at 0.01 %, the particle size distribution is the narrowest, indicating the most homogeneous particle size, with the average particle size of RPAe reaching 370 ± 18 nm. One potential explanation for this phenomenon is that PA alters the spatial structure of the RBP, causing larger protein particles to degrade and form more smaller-sized particles. This results in the formation of a denser particle layer, which reduces the interfacial free energy and leads to the formation of smaller droplets during homogenisation (Harman, Patel, Guldin, & Davies, 2019). However, when the concentration PA is too high, it causes the RBPs to be bridged together, resulting in the occurrence of agglomeration and increase in particle size.

Electrostatic repulsion between charged colloidal particles is the main force in protein stabilized emulsion (Tan et al., 2017). The Zeta-potential of RAe and RPAe was shown in Fig. 1D. The absolute values of the zeta-potential of both Pickering emulsion with PA addition were all higher than the control group without PA. This phenomenon can be attributed to the presence of ionisable phosphate groups in PA, which facilitate interactions with proteins, leading to phosphorylation and an increase of negatively charged groups (Wang et al., 2023). However, when the concentration of the PA is excessive, the intermolecular forces between the protein molecules increase, resulting in a weakening of the electrostatic effect and the shielding of the negative charge (Jiang & Xiong, 2013).

3.1.3. Interfacial protein adsorption

Interfacial protein adsorption in Pickering emulsion prepared by mixing various concentrations of PA is shown in Fig. 1E. The study revealed that as the concentration of PA increased, the adsorption protein initially increased and then subsequently decreased. The reason behind this observation is that the inclusion of PA leads to the unfolding and increased flexibility of RBP's spatial structure, thereby causing the exposure of internal hydrophobic and charged groups on the surface of RBP, making it more favourable for adsorption at the interface (Wang et al., 2012). The increase in interfacially adsorbed proteins not only forms a dense interfacial film, which increases spatial site resistance, but also effectively reduces the interfacial tension between oil and water, leading to a decrease in particle size (Piriyaprasarth, Juttulapa, & Sriamornsak, 2016). However, with the further increase of PA concentration, excess PA may result in the denaturation of RBP, thereby impairing its ability to adsorb at the oil-water interface.

3.1.4. Emulsifying properties

EAI reflects the ability of surfactants to adsorb onto the surface of particles, thus forming and stabilizing Pickering emulsion while lowing interfacial tension at the oil-water interface. Meanwhile, ESI can be described as the strength of the Pickering emulsion to resist separation, indicating its ability to maintain a dispersed state.. The effect of PA concentration on EAI and ESI is shown in Fig. 2A and Fig. 2B. The Pickering emulsion compounded with different concentrations of PA showed an increase in both EAI and ESI compared to the control group that used only RBP ($P < 0.05$). Both the EAI and ESI reached their maximum values when the addition of PA reached 0.01 %. However, the addition of a higher concentration of PA resulted in a decrease in both the EAI and ESI indices of Pickering emulsion. This is consistent with the results of interfacial protein adsorption. Protein adsorption on the surface of oil droplets is a physical adsorption process (Li et al., 2020). The ability of proteins to adsorb is affected by changes in their structure and surface hydrophobicity. Therefore, the surface modification effect of suitable PA concentration resulted in enhanced molecular flexibility of RBP. The side chains and the primary peptide chain of a protein with a flexible structure are in a state of constant motion. As a result, the hydrophobic amino acids that are buried inside the protein molecule will gradually become exposed. The exposure of hydrophobic groups on the protein surface can enhance the spatial resistance between droplets and enhance the adsorption efficiency of the protein at the oil-water interface by lowering the energy barriers.

3.1.5. Oxidative stability

POV and TABRS are important indicators that represent the primary and secondary oxidation products that occur during the oxidation of fats and oils. The oxidative stability of Pickering emulsion is primarily affected by the oxidation and rancidity of oils and fats. The addition of Fe^{2+} mimics transition metal (pro-oxidant) ions that are naturally present in the raw materials of food systems or introduced during processing. As shown in Fig. 3A and Fig. 3B, the addition of PA can

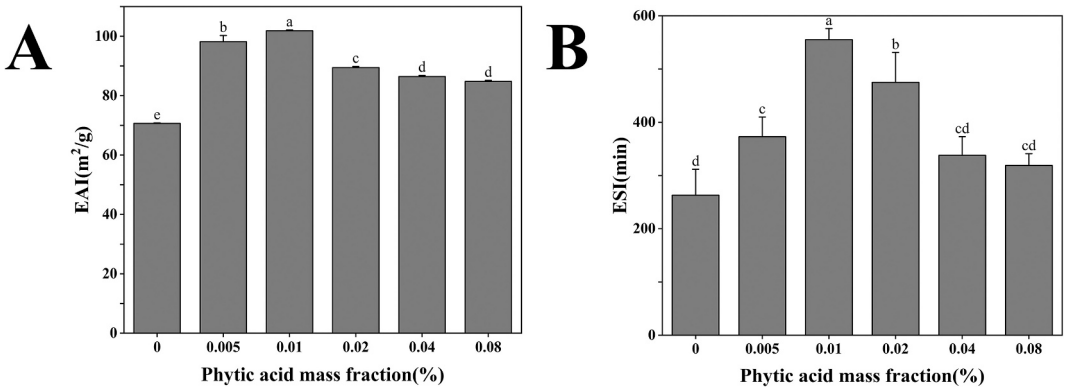

Fig. 2. Emulsifying activity index (EAI) (A), Emulsification stability index (ESI) (B).

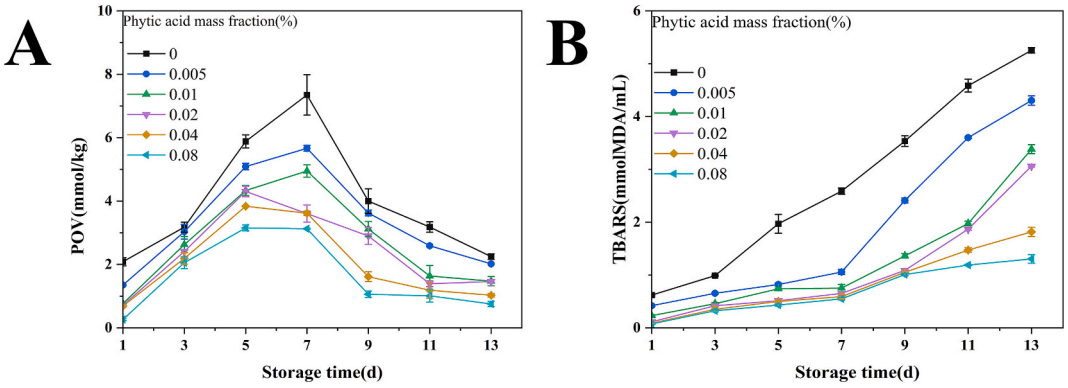

Fig. 3. Peroxide values (POV) (A), Thiobarbituric acid reactive substance (TBARS) (B).

significantly reduce the POV and TABRS of the Pickering emulsion system. According to Fig. 3A, POV reached its peak on day 7 and then decreased, as the process of fat oxidation is characterized by a dynamic equilibrium. Hydroperoxides are produced through the oxidation of oils and fats, but they can also decompose and polymerize. Once the hydroperoxides content reaches a certain level, the rate of decomposition and polymerization accelerates. This phenomenon can also be observed in conjunction with Fig. 3B, where the rate of TABRS production markedly increased on day 7. It can be seen that the incorporation of PA can effectively retard the oxidation of oils in the Pickering emulsion. The oxidation of oils and fats is a chain reaction process involving free radicals, which can be divided into chain initiation, chain propagation, and chain termination. Transition metal ions are involved in the chain initiation process. And PA can retard the oxidation of oils and fats by chelation transition metal ions or free oxygen radicals and hydroxyl radicals generated in the oxidation (Sun, Wang, Chen, & Li, 2011). Furthermore, the addition of PA enhanced the interfacial adsorption content of RBP, resulting in a denser interfacial layer. This may provide a more robust physical barrier to impede the contact of ATBSO with transition metal ions (Pan et al., 2019). The presence of PA mitigates these oxidative processes, suggesting their potential role in improving the oxidative stability of the Pickering emulsion.

3.1.6. *Stability assessment*

3.1.6.1. Effect of pH. The impact of pH on Pickering emulsion stability is illustrated in Fig. 4A. The combination of Pickering emulsion appearance and particle size suggests that the Pickering emulsion's anti-delamination stability is enhanced as pH increases. This is due to the fact that an increase in pH leads to an increase in the absolute value of the zeta potential (Xu et al., 2016), increasing the electrostatic repulsion between the particle molecules, and improving the stability of the

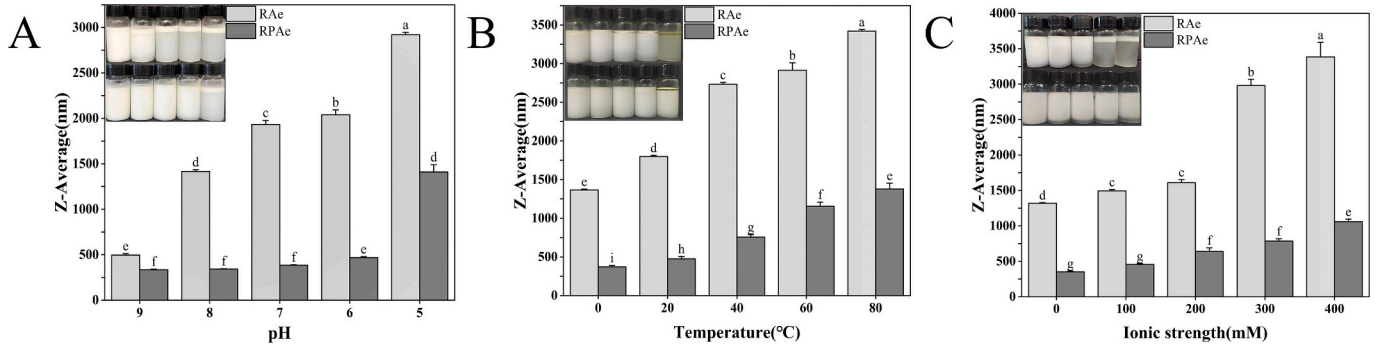

Fig. 4. Effects of environmental conditions on Pickering emulsion stability. pH (A), Temperature (B), NaCl concentration (C).

Pickering emulsion. On the other hand, the solubility of RBP is lowest at pH 4.0 to 5.0 (Rivero Meza et al., 2024). An increase in pH leads to an enhancement in solubility, which in turn decreases the interfacial tension of the Pickering emulsion (Chang, Tu, Ghosh, & Nickerson, 2015). Furthermore, it can also be seen from Fig. 3A that the addition of PA further expands the pH stability range of the Pickering emulsion. This indicates that the chelation of PA and RBP, on the one hand, alters the spatial structure of RBPs, resulting in a reduction in particle size, which consequently increases resistance to gravitational separation and aggregation. On the other hand, the interaction between PA and RBP results in an increase in the absolute value of the zeta potential, which effectively inhibits droplet aggregation (Tcholakova, Denkov, & Lips, 2008).

3.1.6.2. Effect of temperature. The effects of temperature on Pickering emulsion stability is shown in Fig. 4B. RAe demonstrated water-oil separation after heat treatment, while RPAe only showed water-oil separation following treatment at 80 °C. Furthermore, the particle size of the Pickering emulsion increased after the heat treatment. This indicates that heat treatment leads to the aggregation of RBPs, forming particles of a larger size, which is not conducive to their adsorption.. The study by Peng et al. (Peng et al., 2016) also reports that heating treatment affects the adsorption behaviour of proteins. If the droplets are not entirely coated by solid particles to form a stable solid interfacial film, they will be attracted to each other due to van der Waals and other forces, resulting in a certain degree of flocculation or aggregation (Tan, Han, & Yang, 2021). However, the particle size of the RBP was reduced by PA, the interaction between PA and RBP results in a reduction in RBP particle size, which in turn enhances the temperature stability of the Pickering emulsion.

3.1.6.3. Effect of NaCl concentration. The stability of emulsion is influenced by variations in ionic strength (Ortiz, Pochat-Bohatier, Cambedouzou, Bechelany, & Miele, 2020). Fig. 4C illustrates the impact of NaCl concentration on Pickering emulsion stability, where an increase in NaCl concentration leads to a decrease in Pickering emulsion stability. This phenomenon occurs because the carboxylate ion (—COO—) is located at the periphery of the molecule and is highly active in the anionic environment. The addition of NaCl initiates a neutralisation reaction between the carboxylate ion (—COO—) and Na^+, which reduces the negative charge on the surface of the protein. This weakens the electrostatic repulsion between droplets, promoting larger droplet sizes (Dai, Zhou, Wei, Gao, & McClements, 2019; Wang, Li, Wang, Adhikari, & Shi, 2010). However, the PA has a polyphosphate moiety surrounding the central inositol ring, which is capable of strongly chelation with various metal cations (Wang & Guo, 2021), reducing the binding of NaCl and carboxylate ions (-COO-).

3.2. Characterization of particles

3.2.1. Particle morphology analysis

As mentioned earlier, the presence of PA improves the physical and oxidative stability of the RPAe. On the other hand, it may also be that the interaction between PA and RBP enhances the stability of the RPAe, which requires further explanation of the interaction between PA and RBP. Fig. 5 shows the particle morphology of RBP-PA and RBP after freeze-drying. The lyophilised RBP (Fig. 5A) consisted of smooth-surfaced spheroidal particles of varying sizes, with no bonding between the particles. As the concentration of PA increased, the surface of RBP ruptured, and its internal structure gradually unfolded, forming small molecular block structures. Small particle size protein is favourable for adsorption at the interface (Chen et al., 2019). Moreover, During the process of protein coiling and folding, hydrophobic amino acids tend to remain distant from the solvent and remain buried inside the protein molecule. Conversely, polar amino acids tend to be exposed on the surface of the protein molecule, while polar amino acids tend to be exposed on the surface of the RBP molecule, coming into contact with the solvent. This means that some internal hydrophobic groups may be exposed on the surface of the RBP molecule. However, with an increase in PA concentration, some of the molecular structures of RBP became fully unfolded and stacked up, potentially shielding certain hydrophobic sites and making it difficult for the stacked RBP to adsorb onto the particle surface.

3.2.2. Surface hydrophobicity analysis

The extent of surface hydrophobicity is closely related to the type and number of amino acid residues exposed on the surface, as well as the spatial structure of the protein. The exposure of hydrophobic groups facilitates the adsorption of proteins onto the interface, arranging them into a viscoelastic interfacial network structure. This enhances the spatial resistance between particles, thereby improving the emulsion's resistance to creaming (Wang et al., 2012). As demonstrated in Fig. 6, the inclusion of PA resulted in a significant improvement in the surface hydrophobicity of RBP ($P < 0.05$), as the concentration of PA increases

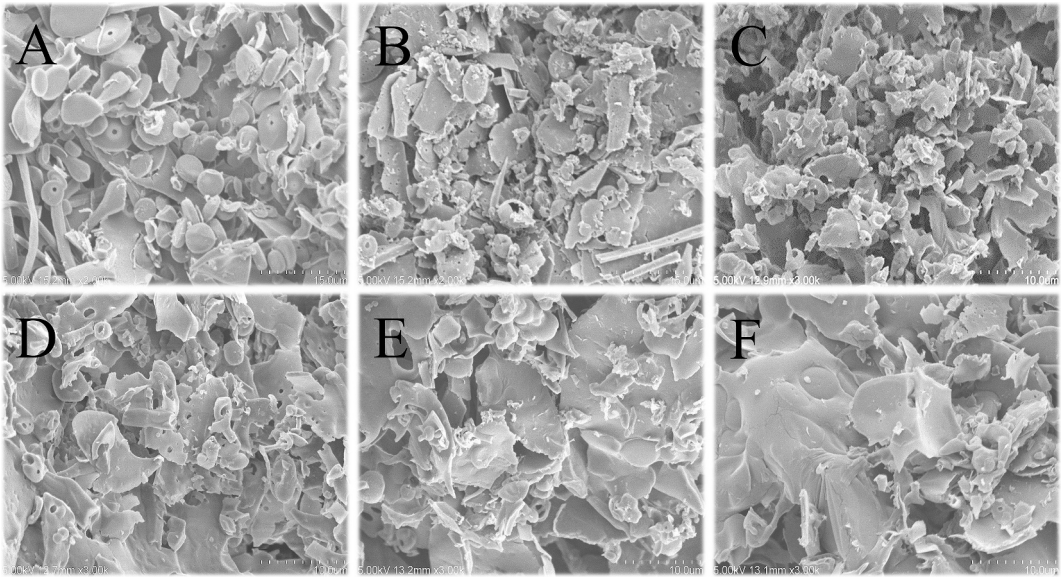

Fig. 5. SEM of RBP complexed with different mass fractions of PA. A ~ F- 0 %, 0.005 %, 0.01 %, 0.02 %, 0.04 %, 0.08 %.

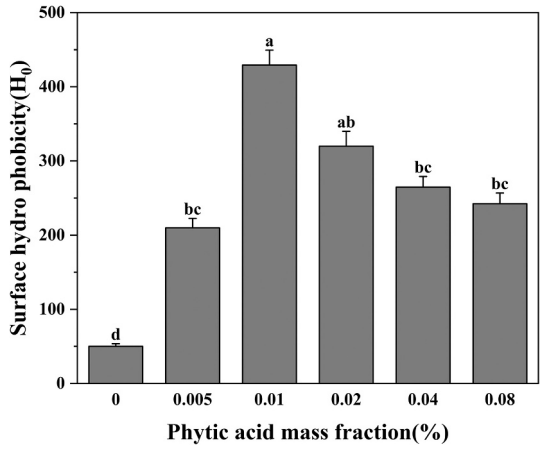

Fig. 6. Surface hydrophobicity of RBP complexed with different mass fractions of PA.

(0.005 %–0.8 %, *w/v*), with a trend of initial increase followed by a decrease. This is related to the fact that PA changes the structure of RBP, leading to the exposure of internal hydrophobic groups as shown by the results of SEM in Fig. 5. At concentrations of PA in excess of 0.01 % (*w/v*), the RBP molecules gradually unfold to form large block structure and stack together, which may shield some of the hydrophobic sites. In addition, hydrophobic groups in excess can also aggregate through hydrophobic binding, causing them to be buried inside the RBP molecule (Li, Wu, & Wu, 2020).

3.2.3. Endogenous fluorescence analysis

To further verify the effect of PA on the molecular structure of RBP, the spectral information of the two was analysed using fluorescence spectroscopy. Changes in the intensity and displacement of the fluorescence peak of endogenous fluorescence of a protein molecule can reflect changes in the structure of the protein, such as unfolding, aggregation or binding to other molecules (Ali, Al-Lohedan, Rafiquee, Atta, & Ezzat, 2015). Fig. 7 illustrates that RBP has a significant fluorescence emission peak at 313 nm. And the fluorescence intensity of RBP decreased as the concentration of PA increased. Furthermore, the introduction of PA caused a slight redshift of the maximum emission peak of RBP, shifting from 313 nm to 314 nm. These findings suggest an interaction between PA and RBP, thereby affecting the polar microenvironment of tyrosine and tryptophan of RBP.

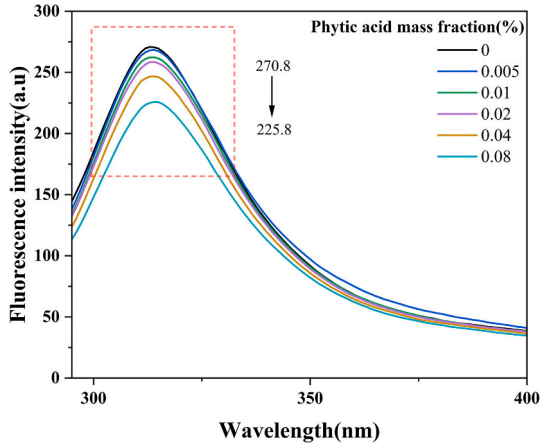

Fig. 7. Endogenous fluorescence of RBP complexed with different mass fractions of PA.

3.2.4. FT-IR spectra analysis

Furthermore, different concentrations of PA and RBP are used to form composite particles to investigate the impact of PA on the chemical structure of RPB through their interaction by FT-IR spectra analysis. Fig. 8A shows the FT-IR spectra of freeze-dried RBP compounded with different concentrations of PA. The protein spectra exhibited prominent peaks at 3400 cm^{-1} (amide A band, representing N—H stretching and O—H stretching), 1650 cm^{-1} (amide I band, representing C—O stretching), and 1540 cm^{-1} (amide II band, representing C—N stretching and N—H bending) (Wang et al., 2020). PA displays four distinct absorption peaks, specifically the stretching vibration of HPO_4^{2-} at 1648 cm^{-1}, and the stretching vibration of the phosphate group at various frequencies ranging from 1202 to 970 cm^{-1} (P═O, 1170 cm^{-1}; C-O-P, 1124 cm^{-1}; PO3, 970 cm^{-1}) (Cui et al., 2008; Gao, Zhang, & Zhang, 2009). The emergence of PA's phosphate group characteristic peaks indicates an interaction between PA and RBP. The absorption peaks in the amide A band of RBP-PA exhibit a red shift as the PA concentration increases. It is attributed to the formation of intermolecular hydrogen bonds, leading to a decrease in the bonding constant and a shift of the absorption peaks towards lower frequencies (Sun et al., 2021). Typically, changes in the infrared spectra of proteins are accompanied by alterations in their secondary structure.

Fig. 8B and **C** demonstrate that primary secondary structure of RBP consists of β-sheet and contains fewer α-helix, similar to many plant proteins (Zhu et al., 2010). As the concentration of PA increased, the number of α-helices in RBP exhibited a trend of initial decline, followed by an upward trajectory. Conversely, the random coil count exhibits an opposite pattern of change. The α-helix structure in protein is stabilized by hydrogen and hydrophobic bonds, respectively (Park, Yang, Lee, & Kim, 2017). This indicates that the interaction between PA and RBP reorganises the distribution of hydrogen and hydrophobic bonds within the protein, subsequently altering its α-helix structural content. Meanwhile, the results demonstrate that the incorporation of an optimal concentration of PA enhances the flexibility of RBP, aligning with the SEM findings. Furthermore, the number of β-sheets in the RBP-PA complex surpasses that in RBP. This is attributed to the alteration of the β-turn angle of the peptide orientation, which promotes protein molecule folding (Zhou, Sun, Qian, Li, & Wang, 2019). The level of protein molecule aggregation is positively correlated with increased β-sheet (Wang, Zou, Gu, & Yang, 2018; Zhou et al., 2019). This indicates that RBP molecules aggregate at high PA concentrations, which subsequently shields some of the hydrophobic sites.

3.2.5. Molecular docking results

To theoretically elucidate the interaction between PA and RPB, we further used molecular docking technology to verify the previous conclusions. The proteins in rice bran are located in the seed coat layer, including the pericarp, tegmen, and aleurone (Rivero Meza et al., 2024). 1RZL is a protein found exclusively in the aleurone layer (Yu, Chung, Fowler, & Suh, 1988). Thus, we selected it as a model protein to simulate the interaction mechanism between RBP and PA. Fig. 9 shows the docking results for 1RZL and PA. The figure illustrates that there are eight amino acid residues surrounding PA, including four hydrophobic residues (Gly30, Pro12, Leu34, and Ala9), one hydrophilic neutral residue (Gln5), and three hydrophilic basic residues (Ser8, 29, 33). Ser primarily interacts with PA through hydrogen bonding. Based on the 3D docking results, it is evident that PA does not penetrate into the protein's hydrophobic cavity, instead it interacts with the amino acid residues on the surface. This is due to the fact that PA has six phosphate groups with tethering ability for O—H, causing it to bind less tightly to amino acid residues, thus creating a significant spatial site-blocking effect. Therefore, the effects of PA on protein structure mainly lie in chelation and spatial conformational changes (Wang et al., 2023).

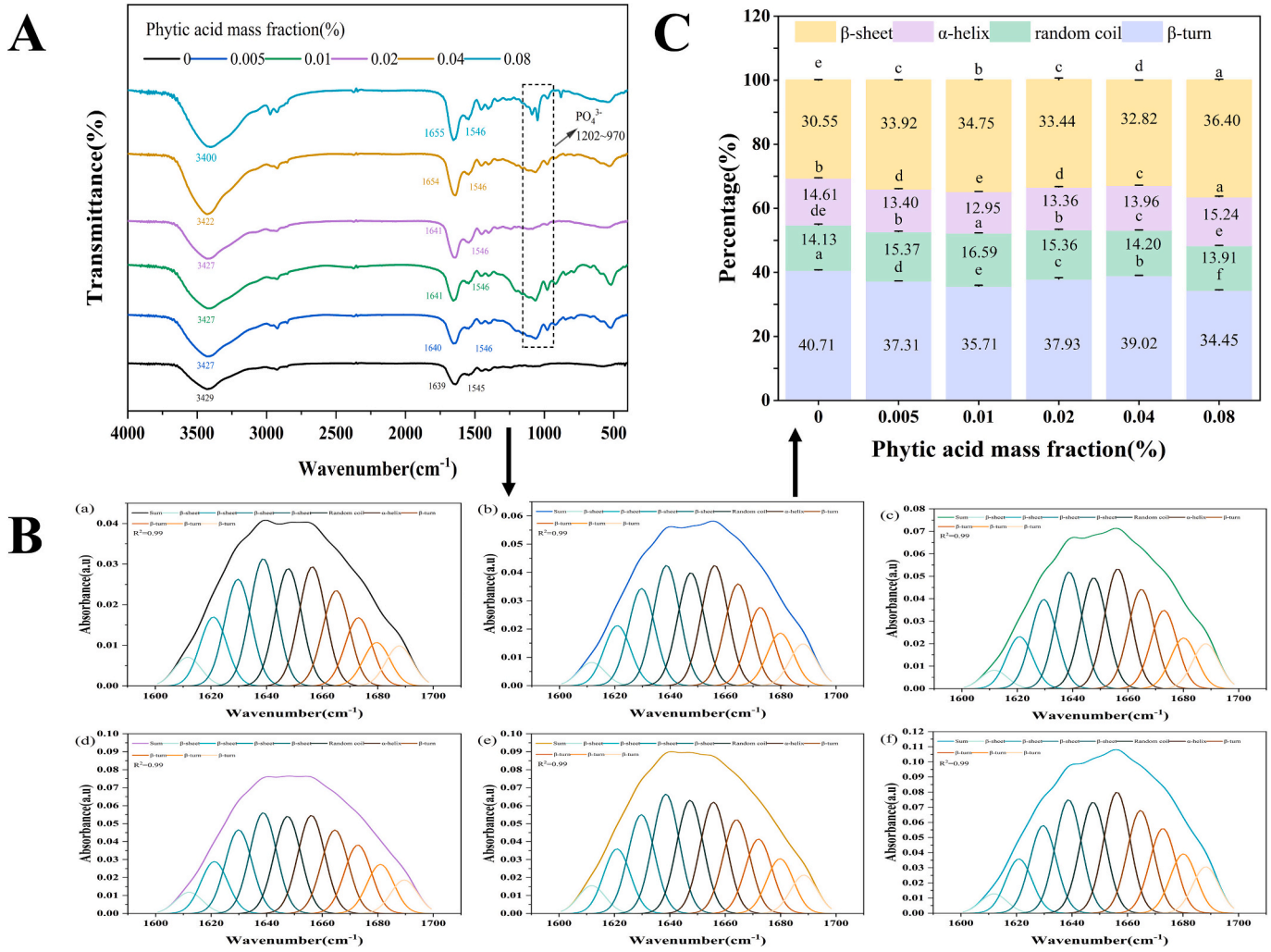

Fig. 8. FT-IR spectra RBP complexed with different mass fractions of PA. (a) ~ (f)- 0 %, 0.005 %, 0.01 %, 0.02 %, 0.04 %, 0.08 %.

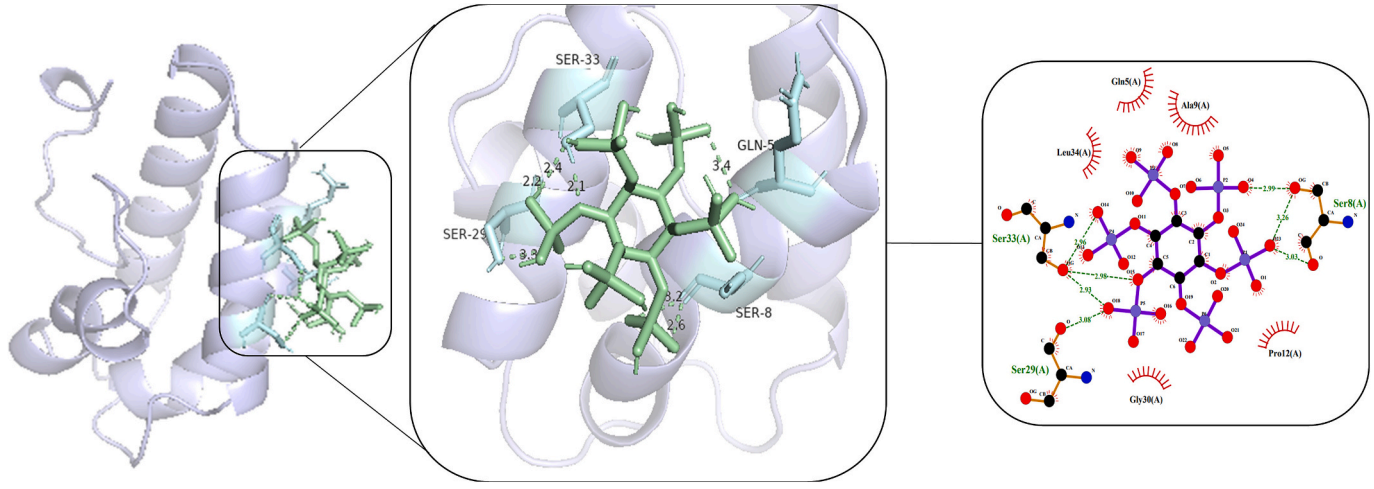

Fig. 9. The 3D and 2D image of 1RZL docking with phytic acid.

4. Conclusion

In conclusion, the Pickering emulsion of *Acer truncatum* Bunge seed oil, modified with PA-treated RBP, exhibits enhanced static stability and lipid oxidation resistance. The incorporation of moderate concentrations (0.01 %, *w/v*) of PA resulted in an increase in the amount of RBP adsorbed at the oil-water interface, leading to the formation of a more compact interfacial film. This is due to the fact that the appropriate concentration of PA facilitates the cleavage of RBP, resulting in the formation of smaller particles and a reduction in the number of rigid

structures, specifically α-helices, while increasing the proportion of surface hydrophobic amino acids. Furthermore, the interaction of PA with RBP results in an increase in the number of negatively charged groups, thereby amplifying electrostatic repulsion between droplets. Nevertheless, when the concentration of PA is in excess of 0.01 % (*w/v*), it results in the aggregation of RBP particles and the shielding of some of the hydrophobic sites, which in turn leads to the destabilisation of the Pickering emulsion. In lipid oxidation experiments, PA displays the capacity to form strong complexes with pro-oxidants (Fe^{2+}), which delays the formation of lipid oxidation products. This study broadens the scope of application for PA and RBP, by-products of rice processing, and offers a theoretical foundation for the promotion of ATBSO in water-soluble foods and pharmaceuticals.

CRediT authorship contribution statement

Jianjun Huang: Writing – original draft, Formal analysis, Data curation. **Ruyi Sha:** Writing – review & editing, Project administration, Funding acquisition. **Jing Dai:** Writing – review & editing. **Zhenzhen Wang:** Supervision. **Min Cai:** Writing – review & editing. **Xianxiu Li:** Writing – review & editing. **Jianwei Mao:** Conceptualization.

Declaration of competing interest

The authors declare that they have no known competing financial interests or personal relationships that could have appeared to influence the work reported in this paper.

Data availability

Data will be made available on request.

Acknowledgement

This work was financially supported by Zhejiang Province “San Nong Jiu Fang” Science and Technology Cooperation Project (2024SNJF012).

References

Ali, M. S., Al-Lohedan, H. A., Rafiquee, M. Z. A., Atta, A. M., & Ezzat, A. O. (2015). Spectroscopic studies on the interaction between novel polyvinylthiol-functionalized silver nanoparticles with lysozyme. *Spectrochimica Acta Part A Molecular & Biomolecular Spectroscopy, 135*, 147–152. https://doi.org/10.1016/j.saa.2014.06.124

Chang, C., Tu, S., Ghosh, S., & Nickerson, M. T. (2015). Effect of pH on the inter-relationships between the physicochemical, interfacial and emulsifying properties for pea, soy, lentil and canola protein isolates. *Food Research International, 77*, 360–367. https://doi.org/10.1016/j.foodres.2015.08.012

Chen, W. P., Liang, G. J., Li, X., He, Z. Y., Zeng, M. M., Gao, D. M., … Chen, J. (2019). Impact of soy proteins, hydrolysates and monoglycerides at the oil/water interface in emulsions on interfacial properties and emulsion stability. *Colloids and Surfaces. B, Biointerfaces, 177*, 550–558. https://doi.org/10.1016/j.colsurfb.2019.02.020

Chen, W. Q., Ding, Y. H., Zhao, Y. M., & Ma, H. L. (2023). Strategies to improve the emulsification properties of rice proteins as a promising source of plant-based emulsifiers: An updated mini-review. *Food Bioscience, 53*. https://doi.org/10.1016/j.fbio.2023.102697

Cui, S., McClements, D. J., Shi, J., Xu, X., Ning, F., Liu, C., … Dai, L. (2023). Fabrication and characterization of low-fat Pickering emulsion gels stabilized by zein/phytic acid complex nanoparticles. *Food Chemistry, 402*, Article 134179. https://doi.org/10.1016/j.foodchem.2022.134179

Cui, X., Li, Q., Li, Y., Wang, F., Jin, G., & Ding, M. (2008). Microstructure and corrosion resistance of phytic acid conversion coatings for magnesium alloy. *Applied Surface Science, 255*(5p1), 2098–2103. https://doi.org/10.1016/j.apsusc.2008.06.199

Dai, L., Zhou, H., Wei, Y., Gao, Y., & McClements, D. J. (2019). Curcumin encapsulation in zein-rhamnolipid composite nanoparticles using a pH-driven method. *Food Hydrocolloids, 93*, 342–350. https://doi.org/10.1016/j.foodhyd.2019.02.041

Gao, L., Zhang, C., & Zhang, M. (2009). Phytic acid conversion coating on mg-Li alloy. *Journal of Alloys and Compounds: An Interdisciplinary Journal of Materials Science and Solid-state Chemistry and Physics, 1/2*, 485. https://doi.org/10.1016/j.jallcom.2009.06.089

Guo, Q., Cui, B., Yuan, C., Guo, L., Li, Z., Chai, Q., Wang, N., Gänzle, M., & Zhao, M. (2024). Fabrication of dry S/O/W microcapsule and its probiotic protection against different stresses. *Journal of the Science of Food and Agriculture, 104*(5), 2842–2850. https://doi.org/10.1002/jsfa.13175

Harman, C. L. G., Patel, M. A., Guldin, S., & Davies, G.-L. (2019). Recent developments in Pickering emulsions for biomedical applications. *Current Opinion in Colloid & Interface Science, 39*, 173–189. https://doi.org/10.1016/j.cocis.2019.01.017

Jiang, J., & Xiong, Y. L. (2013). Extreme pH treatments enhance the structure-reinforcement role of soy protein isolate and its emulsions in pork myofibrillar protein gels in the presence of microbial transglutaminase. *Meat Science, 93*(3), 469–476. https://doi.org/10.1016/j.meatsci.2012.11.002

Li, D., Zhao, Y., Wang, X., Tang, H. L., Wu, N., Wu, F., … Elfalleh, W. (2020). Effects of (+)-catechin on a rice bran protein oil-in-water emulsion: Droplet size, zeta-potential, emulsifying properties, and rheological behavior. *Food Hydrocolloids, 98*(Jan.), 98. https://doi.org/10.1016/j.foodhyd.2019.105306

Li, F., Wu, X. J., & Wu, W. (2020). Effects of malondialdehyde-induced protein oxidation on the structural characteristics of rice protein. *International Journal of Food Science & Technology, 55*(2), 760–768. https://doi.org/10.1111/ijfs.14379

Li, Q., Chen, J., Yu, X., & Gao, J.-M. (2019). A mini review of nervonic acid: Source, production, and biological functions. *Food Chemistry, 301*, Article 125286. https://doi.org/10.1016/j.foodchem.2019.125286

Li, Z., Liang, J., Lu, L., Liu, L., & Wang, L. (2024). Effect of ferulic acid incorporation on structural, rheological, and digestive properties of hot-extrusion 3D-printed rice starch. *International Journal of Biological Macromolecules, 266*, Article 131279. https://doi.org/10.1016/j.ijbiomac.2024.131279

Ortiz, D. G., Pochat-Bohatier, C., Cambedouzou, J., Bechelany, M., & Miele, P. (2020). Current trends in Pickering emulsions: Particle morphology and applications. *Engineering, 6*(4), 468–482. https://doi.org/10.1016/j.eng.2019.08.017

Pan, X., Fang, Y., Wang, L. L., Shi, Y., Xie, M. H., Xia, J., … Hu, Q. H. (2019). Covalent interaction between Rice protein hydrolysates and Chlorogenic acid: Improving the stability of oil-in-water emulsions. *Journal of Agricultural and Food Chemistry, 67*(14), 4023–4030. https://doi.org/10.1021/acs.jafc.8b06898

Park, C. W., Yang, H.-M., Lee, K. S., & Kim, J.-D. (2017). Disulfide and β-sheet stabilized poly(amino acid) nanovesicles for intracellular drug delivery. *Journal of Industrial and Engineering Chemistry, 56*, 277–284. https://doi.org/10.1016/j.jiec.2017.07.020

Pei, Y. Q., Deng, Q. C., McClements, D. J., Li, J., & Li, B. (2020). Impact of Phytic acid on the physical and oxidative stability of protein-stabilized oil-in-water emulsions. *Food Biophysics, 15*(4), 433–441. https://doi.org/10.1007/s11483-020-09641-z

Peng, W., Kong, X., Chen, Y., Zhang, C., Yang, Y., & Hua, Y. (2016). Effects of heat treatment on the emulsifying properties of pea proteins. *Food Hydrocolloids, 52*, 301–310. https://doi.org/10.1016/j.foodhyd.2015.06.025

Piriyaprasarth, S., Juttulapa, M., & Sriamornsak, P. (2016). Stability of rice bran oil-in-water emulsions stabilized by pectin-zein complexes: Effect of composition and order of mixing. *Food Hydrocolloids, 61*, 589–598. https://doi.org/10.1016/j.foodhyd.2016.06.015

Qi, Y., Huang, Y., Dong, Y., Zhang, W., Xia, F., Bai, H., … Shi, L. (2023). Effective improvement of the oxidative stability of *Acer truncatum* Bunge seed oil, a new Woody oil food resource, by rosemary extract. *Antioxidants, 12*. https://doi.org/10.3390/antiox12040889

Qiao, Q., Wang, X., Ren, H., An, K., Feng, Z., Cheng, T., & Sun, Z. (2019). Oil content and Nervonic acid content of *Acer truncatum* seeds from 14 regions in China. *Horticultural Plant Journal, 5*(01), 24–30. https://doi.org/10.1016/j.hpj.2018.11.001

Rivero Meza, S. L., Cañizares, L., Dannenberg, B., Peres, B. B., Rodrigues, L. A., Mardade, C., … de Oliveira, M. (2024). Sustainable rice bran protein: Composition, extraction, quality properties and applications. *Trends in Food Science & Technology, 145*, Article 104355. https://doi.org/10.1016/j.tifs.2024.104355

Sun, L. H., Lv, S. W., Chen, C. H., & Wang, C. (2019). Preparation and characterization of rice bran protein-stabilized emulsion by using ultrasound homogenization. *Cereal Chemistry, 96*(3), 478–486. https://doi.org/10.1002/cche.10147

Sun, Y. E., Wang, W. D., Chen, H. W., & Li, C. (2011). Autoxidation of unsaturated lipids in food emulsion. *Critical Reviews in Food Science and Nutrition, 51*(5), 453–466. https://doi.org/10.1080/10408391003672086

Sun, Y. F., Zhang, S., Xie, F. Y., Zhong, M. M., Jiang, L. Z., Qi, B. K., & Li, Y. (2021). Effects of covalent modification with epigallocatechin-3-gallate on oleosin structure and ability to stabilize artificial oil body emulsions. *Food Chemistry, 341*(Pt 2), Article 128272. https://doi.org/10.1016/j.foodchem.2020.128272

Tan, H., Han, L., & Yang, C. (2021). Effect of oil type and β-carotene incorporation on the properties of gelatin nanoparticle-stabilized Pickering emulsions. *LWT, 141*, Article 110903. https://doi.org/10.1016/j.lwt.2021.110903

Tan, Y., Deng, X., Liu, T., Yang, B., Zhao, M., & Zhao, Q. (2017). Influence of NaCl on the oil/water interfacial and emulsifying properties of walnut protein-xanthan gum. *Food Hydrocolloids, 72*, 73–80. https://doi.org/10.1016/j.foodhyd.2017.05.031

Tcholakova, S., Denkov, N. D., & Lips, A. (2008). Comparison of solid particles, globular proteins and surfactants as emulsifiers. *Physical Chemistry Chemical Physics, 10*(12), 1608–1627. https://doi.org/10.1039/b715933c

Wang, B., Li, D., Wang, L.-J., Adhikari, B., & Shi, J. (2010). Ability of flaxseed and soybean protein concentrates to stabilize oil-in-water emulsions. *Journal of Food Engineering, 100*(3), 417–426. https://doi.org/10.1016/j.jfoodeng.2010.04.026

Wang, H., Chen, L., Wu, S., Jin, W., Shen, W., Hu, Z., … Liu, G. (2023). Improve stability and application of rice oil bodies via surface modification with ferulic acid, (−)-epicatechin, and phytic acid. *Food Chemistry, 409*, Article 135274. https://doi.org/10.1016/j.foodchem.2022.135274

Wang, J. M., Xia, N., Yang, X. Q., Yin, S. W., Qi, J. R., He, X. T., … Wang, L. J. (2012). Adsorption and dilatational rheology of heat-treated soy protein at the oil-water interface: Relationship to structural properties. *Journal of Agricultural and Food Chemistry, 60*(12), 3302–3310. https://doi.org/10.1021/jf205128v

Wang, P., Zou, M., Gu, Z., & Yang, R. (2018). Heat-induced polymerization behavior variation of frozen-stored gluten. *Food Chemistry, 255*, 242–251. https://doi.org/10.1016/j.foodchem.2018.02.047

Wang, R., & Guo, S. (2021). Phytic acid and its interactions: Contributions to protein functionality, food processing, and safety. *Comprehensive Reviews in Food Science and Food Safety, 20*(2), 2081–2105. https://doi.org/10.1111/1541-4337.12714

Wang, W. D., Li, C., Bin, Z., Huang, Q., You, L. J., Chen, C., … Liu, R. H. (2020). Physicochemical properties and bioactivity of whey protein isolate-inulin conjugates obtained by Maillard reaction. *International Journal of Biological Macromolecules, 150*, 326–335. https://doi.org/10.1016/j.ijbiomac.2020.02.086

Xie, D., Deng, F., Shu, J., Zhu, C., Hu, X., Luo, S., & Liu, C. (2022). Impact of the frying temperature on protein structures and physico-chemical characteristics of fried surimi. *International Journal of Food Science & Technology*. https://doi.org/10.1111/ijfs.15741

Xu, X., Zhong, J., Chen, J., Liu, C., Luo, L., Luo, S., … McClements, D. J. (2016). Effectiveness of partially hydrolyzed rice glutelin as a food emulsifier: Comparison to whey protein. *Food Chemistry, 213*, 700–707. https://doi.org/10.1016/j.foodchem.2016.07.047

Yan, X. J., Ma, C. C., Cui, F. Z., McClements, D. J., Liu, X. B., & Liu, F. G. (2020). Protein-stabilized Pickering emulsions: Formation, stability, properties, and applications in foods. *Trends in Food Science & Technology, 103*(1), 293–303. https://doi.org/10.1016/j.tifs.2020.07.005

Yang, R., Zhang, L., Li, P., Yu, L., & Zhang, Q. (2018). A review of chemical composition and nutritional properties of minor vegetable oils in China. *Trends in Food Science & Technology, 74*, 26–32. https://doi.org/10.1016/j.tifs.2018.01.013

Yu, Y. G., Chung, C. H., Fowler, A., & Suh, S. W. (1988). Amino acid sequence of a probable amylase/protease inhibitor from rice seeds. *Archives of Biochemistry and Biophysics, 265*(2), 466–475. https://doi.org/10.1016/0003-9861(88)90151-8

Zhang, T., Xu, J., Chen, J., Wang, Z., Wang, X., & Zhong, J. (2021). Protein nanoparticles for Pickering emulsions: A comprehensive review on their shapes, preparation methods, and modification methods. *Trends in Food Science & Technology, 113*, 26–41. https://doi.org/10.1016/j.tifs.2021.04.054

Zhou, R., Sun, J., Qian, H., Li, Y., & Wang, L. (2019). Effect of the frying process on the properties of gluten protein of you-tiao. *Food Chemistry, 310*, Article 125973. https://doi.org/10.1016/j.foodchem.2019.125973

Zhu, K. X., Sun, R. H., Chen, R. C., Peng, R., Qian, R. F., & Zhou, R. M. (2010). Comparison of functional properties and secondary structures of defatted wheat germ proteins separated by reverse micelles and alkaline extraction and isoelectric precipitation. *Food Chemistry, 123*(4), 1163–1169. https://doi.org/10.1016/j.foodchem.2010.05.081